Heliyon 9 (2023) e15063

Contents lists available at ScienceDirect

Heliyon

journal homepage: www.cell.com/heliyon

Original article

Cork: Enabler of sustainable and efficient coaxial structural batteries

Mafalda Valente [a,b,c], Sara Magalhães Silva [d,e], Maria Helena Braga [b,c,f,*]

[a] Metallurgical and Materials Engineering Department, Engineering Faculty, University of Porto, R. Dr. Roberto Frias s/n, 4200-465 Porto, Portugal
[b] Engineering Physics Department, Engineering Faculty, University of Porto, R. Dr. Roberto Frias s/n, 4200-465 Porto, Portugal
[c] Materials for Energy Research, MaTER Laboratory, Engineering Faculty, University of Porto, R. Dr. Roberto Frias s/n, 4200-465 Porto, Portugal
[d] Amorim Cork Composites, R. Comendador Américo Ferreira Amorim 260, 4535-186 Mozelos, Portugal
[e] EMaRT Group – Emerging: Materials, Research, Technology, ESAN - University of Aveiro, Estrada do Cercal, 449, 3720-509 Oliveira de Azeméis, Portugal
[f] LAETA-INEGI, Institute of Science and Innovation in Mechanical and Industrial Engineering, 4200-465 Porto, Portugal

ARTICLE INFO

Keywords:
Structural batteries
Electrode-less batteries
Cork dielectric
Ferroelectrics
Solid electrolytes

ABSTRACT

Structural batteries aim to advance to 'massless' energy storage units. Here we report an electrode-less coaxial battery with a cork-internal shell, CFRP(+)/cork/Cu/$Na_{2.99}Ba_{0.005}ClO$/Al(−), where CFRP is carbon fiber reinforced polymer. The cell may, alternatively, solely have a cork external shell cork/Cu(+)/$Na_{2.99}Ba_{0.005}ClO$/Al(−). Cork is a cellular material with a negative CO_2 footprint, light, elastic, impermeable to gases or liquids, and an excellent thermal insulator. Cork was used tandemly with a CFRP shell, working as the positive current collector to enhance the structural batteries' properties while allowing a giant electrostatic performance in conjunction with the Na^+ solid-state ferroelectric injected between the Al negative collector and the cork. Cork was shown a polar dielectric. This 'minimalist' cell may perform without copper making the cells even more sustainable. Neither cells contain traditional electrodes, only one or two current collectors. The cells perform from 0 to >50 °C. The maximum capacity of the cork/Cu(+)/$Na_{2.99}Ba_{0.005}ClO$/Al(−) cells is ~110 mAh.cm^{-2} (outer shell) with $\langle I \rangle \approx 90$ μA cm^{-2}, $\langle V \rangle \approx 0.90$ V, $V_{max} \approx 1.1$–1.3 V, $I_{max} \approx 108$ μA cm^{-2}, and a constant resistance discharging life (>40 days). The novel family of cells presented may also harvest waste heat and thermal energy at a constant temperature as their potential and current increase with temperature. Conversely, rising potentials boost the cells' temperature, as expected from pyroelectrics, as shown herein.

1. Introduction

The design and development of new materials strive to meet the user's needs, and materials have paced the evolution of technology for years [1]. The development of renewable energy sources, such as wind, solar, and waves, has become imperative due to the limited resource constraints of traditional fossil fuels [2]. Four main goals upturn when envisioning the perfect battery to become the next-generation powerhouse: **(1)** it should have a high energy density and **(2)** store it safely, **(3)** use environmentally friendly materials and methods, and **(4)** be widely available and inexpensive. The latter goals depend heavily on the electrolyte used [2,3]. To achieve

* Corresponding author. Engineering Physics Department, Engineering Faculty, University of Porto, R. Dr. Roberto Frias s/n, 4200-465 Porto, Portugal.
E-mail address: mbraga@fe.up.pt (M.H. Braga).

https://doi.org/10.1016/j.heliyon.2023.e15063
Received 4 March 2023; Received in revised form 21 March 2023; Accepted 27 March 2023
Available online 8 April 2023

those objectives, research has turned to all-solid-state batteries, potentially safer than those using a liquid with flammable solvents in the electrolyte formula. Likewise, they have proven to allow for a high energy density by permitting electrode pairs with a higher capacity [4]. Although electrolytes such Li_6PS_5Cl, in Li–S cells, are highly expensive and hygroscopic and can only be handled in the glovebox as they may release H_2S, they only enable cells' capacities of ~8 mAh.cm^{-2} (first cycle, I = 44 μA cm^{-2}) for plateau potential of 1.3 V [5] or even less a capacity of ~1.3 mAh.cm^{-2} (cutoff 0.5 V) [6], calling for innovative solutions.

The inorganic solid-state electrolytes of the $A_{3-2x}M_xClO$ (A = Li, Na, K, and M = Mg, …, Ba) family may turn into powders and form composites with polymers such as Polyvinyl acetate PVAc, facilitating their placement on the battery cell suitable for flexible battery design. A fundamental characteristic of using these electrolytes in batteries is that they display an obvious conductivity advantage compared to other solid electrolytes. These electrolytes do not require an additional containment or separator, possess better thermal/chemical stabilities, and have higher mechanical strength [7,8]. They also exhibit a huge dielectric constant (10^7-10^9) over a wide temperature range. This is critical for their application in multifunction systems, specifically in systems working under extreme conditions, such as expected for structural batteries [7].

The ionic movement, leading to polarization, is co-responsible for energy storage in the ferroelectric solid-state cell [8,9]. In typical conditions, the electrolyte should be an electrical insulator to avoid leakage of electrons through the battery's inner cell, propitiating spurious reactions such as those leading to forming a solid electrolyte interphase layer, SEI. Here the Na^+ ferroelectric electrolyte remains a bulk insulator, but the surface electrical conductivity is coadjutant and essential to the unusual behavior of these coaxial structural batteries. A significant step toward developing Na^+-based batteries is enhancing the ionic conductivity in the electrolyte since it propitiates higher polarization and faster and more efficient plating on electrodes-collectors. The no flammability and improved durability broaden their high-performance applications [2,10]. Sodium-ion-based ferroelectric $Na_{2.99}Ba_{0.005}ClO$ electrolytes [4,9,11] have proven essential in the structural cells illustrated in Fig. 1(a–d).

Conversely to the ferroelectric $A_{3-2x}M_xClO$ electrolytes, which are hygroscopic, cork is hydrophobic [12–15]. Cork is also impermeable, thermally insulating, and a fire retardant material, which makes it ideal as a protective battery shell. Another crucial fact is that cork is one of the most sustainable materials as it has a negative carbon footprint; cork can absorb −73 tons of CO_2 per ton of oak tree-extracted cork [16]. All these reasons validate the cork usage as a shell and structural material in batteries. Still, herein we present a new role for cork that, to the best of our knowledge, was never demonstrated before. However, cork was suggested to be used as a sensor, or an antenna, e.g., RFID sensors [14,17,18].

We present cork as a dielectric, enabling colossal electrostatic phenomenon through ≥4.2 mm thick tandem dielectric-conductor-ferroelectric, Fig. 1(a–c), or dielectric-ferroelectric, Fig. 1d. Another functional feature of cork, reported by Mano et al. [19], is its glass transition at 18 °C with low activation enthalpy and entropy and showing a compensation behavior, demonstrating a high degree of cooperativity attributed to a glass-transition-like relaxation process. The existence of a dipolar discharge in the cork with these features

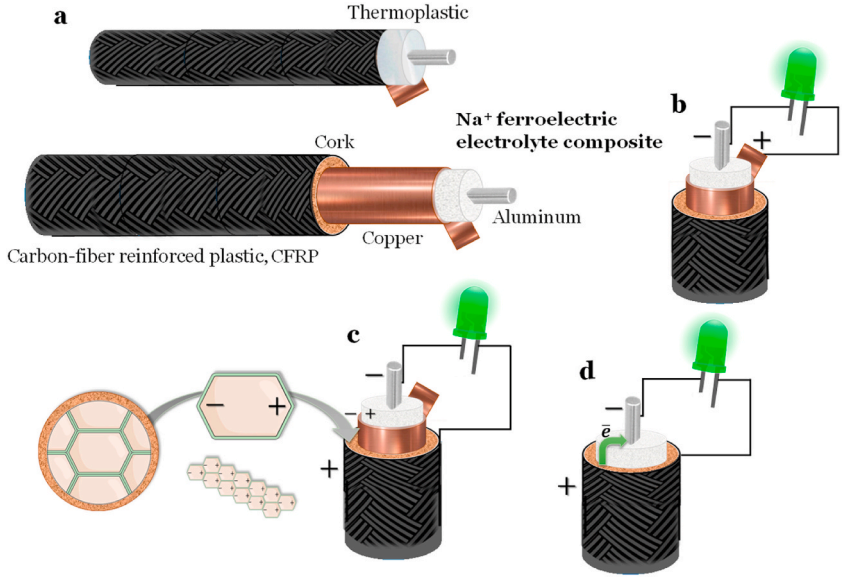

Fig. 1. Illustrates the three possible configurations for the Na^+ ferroelectric electrolyte-based coaxial structural batteries using an internal cork shell (A1, A2) that may function as a dielectric; **a** shows all the external and inner constituents of the cell; **b** CFRP/cork/Cu(+)/$Na_{2.99}Ba_{0.005}ClO$/Al(−) standard electrode-less coaxial cell; **c** CFRP(+)/cork/Cu/$Na_{2.99}Ba_{0.005}ClO$/Al(−) coaxial cell with the CFRP as the positive collector enabled by the surface chemical potential of Cu higher than the CFRP and the $Na_{2.99}Ba_{0.005}ClO$ ferroelectric and topologic character; and **d** CFRP(+)/cork/$Na_{2.99}Ba_{0.005}ClO$ composite/Al(−) coaxial cell with CFRP as the positive collector and the topologic conduction of electrons in the $Na_{2.99}Ba_{0.005}ClO$ electrolyte enabling lighting an LED between the Al negative electrode and the CFRP positive electrode through the dielectric cork; cork and $Na_{2.99}Ba_{0.005}ClO$ electrolyte are two extremely thick dielectrics in series (cork = 1.2 mm and $Na_{2.99}Ba_{0.005}ClO$ ≈ 3 mm thick) that connect with the negative and positive collectors electrostatically.

is similar to poly(n-hexyl isocyanate) rigid chain rod-like polymer and is determinant for its role in the present application [19].

In today's electric transport modes and consumer goods, batteries comprise a large part of the system's weight without fulfilling any structural and load-bearing function. Several studies have recently explored extending batteries' functionalities to incorporate more than one primary function [3,20,21]. An excellent opportunity to overcome this problem is offered using multifunctional systems and materials, especially structural power composites [22–24]. The total system mass and volume can then be reduced, improving the system's overall efficiency [25,26].

Herein we report efficient electrode-less coaxial structural batteries with a ferroelectric $Na_{2.99}Ba_{0.005}ClO$ electrolyte with protective cork shells and with cork-$Na_{2.99}Ba_{0.005}ClO$ tandem dielectric enabling the presence of a single electrode-collector while avoiding the use of copper or other less abundant materials. The cork was reinforced with a carbon fiber-reinforced plastic (CFRP) shell to enhance the coaxial beam-like structural properties while allowing a giant electrostatic performance. The positive current collector is a bifunctional material such as copper Cu(+) or, enabled by the cork, just CFRP(+), associating to being a positive collector, enhanced mechanical properties.

The ferroelectric electrolyte $Na_{2.99}Ba_{0.005}ClO$ with a dielectric constant $\varepsilon_r \approx 10^8$ (40 °C) in series with the cork $\varepsilon_r \approx 1.6$ (40 °C) accounts for almost nothing for the dielectric constant of the full cell when the circuit is closed with the CFRP(+) as the positive collector and the aluminum Al(−) as the negative. However, the topologic conduction in the ferroelectric electrolyte is paramount for establishing a CFRP(+)/cork/$Na_{2.99}Ba_{0.005}ClO$/Al(−) efficient cell. The electrolyte can harvest and store electrical energy within electrodeless cells and self-cycle its output potential and temperature. Harvesting can occur at a constant temperature, making these cells promising as industrial waste thermal and heat collectors and applicable in vehicles, housing, and microgrids. We show a maximum capacity of the electrolyte of 510 mAh.$g^{-1}_{\text{ferroelectric-electrolyte}}$ at 42–44 °C (sand-bath) for a cutoff potential of 0.4 V, corresponding to 76% of the theoretical capacity of 674 mAh.$g^{-1}_{\text{ferroelectric-electrolyte}}$ and an average output current of ≈2 mA (>357 μA cm^{-2}).

In a ferroelectric electrolyte, it is not expected that more than the free ions in $Na^+Cl^-(Na_{1.99}Ba_{0.005}O)$ (35 wt%) will plate on the collectors as the polarization attributed to $(-O-Na-)^-_n$ must compensate for the difference in Fermi levels of the electrode collectors. Although the polarization of $(-O-Na-)^-_n$ will also contribute to the potential difference; it is expected that the positive feedback from the electrical topologic conduction in the ferroelectric also contributes to the coaxial cells' capacity. The cells show open circuit voltages of 1.2254 V for CFRP/cork/Cu(+)/$Na_{2.99}Ba_{0.005}ClO$/Al(−), 1.2457 V for CFRP (+)/cork/$Na_{2.99}Ba_{0.005}ClO$/Al(−), and 1.2474 V for CFRP(+)/cork/Cu/$Na_{2.99}Ba_{0.005}ClO$/Al(−) and light LEDs. The surface chemical potential of the cork was determined to be 0.18 V (SHE) or −4.62 eV (E = 0 eV, electrons at rest in vacuum), reaffirming its polar dielectric and a more positive character than copper.

2. Results and discussion

The materials and cells were prepared as described in Supplementary Information SI Materials and Methods [27–40]. As shown hereafter, the cork's cell structure is prone to polarize in rod chains, as discussed previously. Cork is a great natural material for moisture and extreme temperature protection, with cells with five and six facets [27], as observed in Fig. 2(a and b). However, as introduced herein, this structure may become multifunctional in energy harvesting and storage devices. It is shown that not only may the cork perform as a thermal and moister insulator but also function as a dielectric, polarized by the current in the Cu electrode-collector but also as a tandem dielectric-ferroelectric, enabled by the surface (topologic) current in the $Na_{2.99}Ba_{0.005}ClO$ ferroelectric-electrolyte (Fig. 1d).

The cork shows a surface chemical potential that is very stable, approximately 0.18 V (SHE), −4.62 eV (E = 0 eV, electrons at rest in vacuum), and more positive than the copper tape Fig. 3(a–d). The surface chemical potential is much flatter than the surface's topology (Fig. 3a), which may vary ~400 μm in depth along a length of 3 mm. Impurities may also be observed in the cork by SKP in Fig. 3(b and c), which may facilitate the polarization of the cork. The internal resistance at the interface Cu/cork does not seem significant, with a smooth variation of the surface chemical potential not indicative of quantum square potential barriers or wells observed in oxides and electrolytes [28].

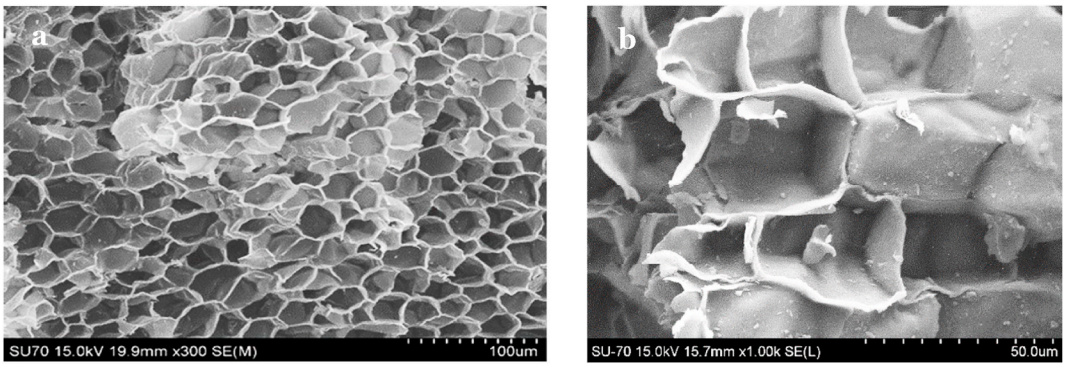

Fig. 2. SEM micrographs of natural cork sputter-coated with Au/Pd; a Magnification × 300. b Magnification × 1000. Secondary electrons with 15.0 keV.

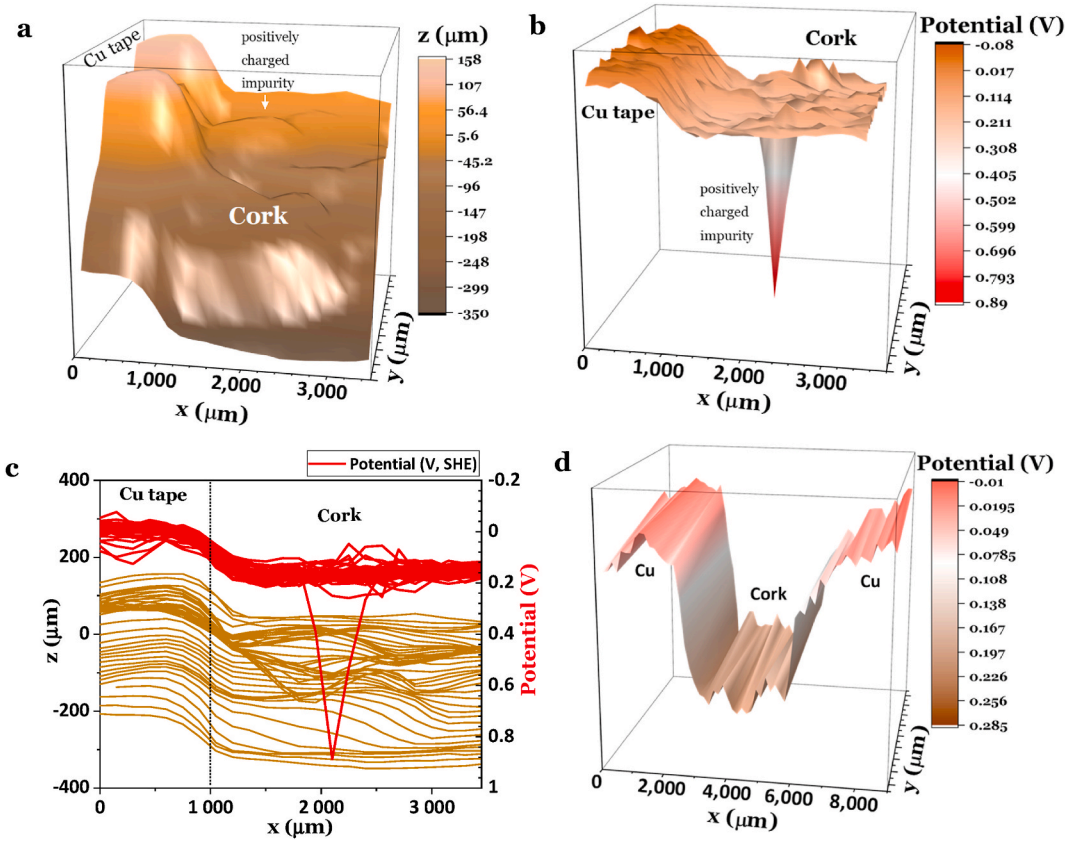

Fig. 3. Topography and surface chemical potential characterization of two copper/cork heterojunctions; a to c capacitive tracking measurement CTM and scanning kelvin probe SKP [40] showing the topography and surface chemical potentials of the Cu-tape and cork of the same heterojunction; The cork shows an impurity charged positively; d surface chemical potential of another Cu-cork-Cu heterojunction showing similar values for the potentials as b and c.

One of the key factors mentioned previously is the high relative permittivity or dielectric constant of the Na^{+}-based solid electrolyte. When developing an energy storage system, permittivity is crucial since it measures the ability to polarize and, therefore, to store electrical energy under the influence of an electric field.

If a ferroelectric with a huge dielectric constant is associated in series with yet another dielectric with a much smaller permittivity, the dielectric constant of the system depends almost only on the smaller dielectric constant, as shown in SI, Eqs. (1) to (4).

The cork's dielectric constant was determined using a symmetric cell Cu/cork layer/Cu at 40 °C and performing EIS. One of the correspondents' Nyqvist plots is shown in SI, Fig. S2a, and the corresponding dielectric constants and ionic conductivities are shown in Table 1.

As shown in Refs. [3,28,29], the dielectric constant or relative real permittivity remains huge when the electrochemical system $Cu/Na_{2.99}Ba_{0.005}ClO/Al$ is placed inside a CFRP shell. By performing cyclic voltammetry CV, the value of the calculated permittivity is demonstrated to be 3.1×10^{8} at 40 °C, with $dV/dt = 1$ mV s^{-1}. In comparison, the coaxial battery with the cork film shows a relative real permittivity of 3.8×10^{8} (SI, Fig. S2b); the permittivity remains in values of the same order of magnitude, which means that it is slightly positively affected by the addition of the cork film to the interior of the structure while functioning just as a shell.

Table 1
Technical information of the cork sheets. Details in SI.

	A1 (ETP050)	A2 (ETP009)	Cork [27,41–43]
Density ($kg.m^{-3}$)	448–512	320	–
Thermal conductivity ($W.m^{-1}.K^{-1}$)	0.062	–	0.040–0.045
Dielectric constant	1.6 (40 °C, this work)	1.3 (40 °C, this work)	~1.3 (~3 GHz) [17,18]
Dielectric strength ($MV.m^{-1}$)	4.3 ± 0.1	–	–
Supported heating rate, $\frac{\Delta T}{\Delta t}$ ($°C.min^{-1}$)	33.0 ± 1.1	23.4 ± 3.1	–
Electrical conductivity ($S.m^{-1}$)	–	–	2.9×10^{-14}
Ionic conductivity ($S.m^{-1}$)	9.6×10^{-8} (40 °C, this work)	1.8×10^{-11} (40 °C, this work)	–

From the analysis of the results of EIS (SI, Tables S1–S3), obtained using Eqs. (1) and (2), three main comparisons are established between **(1)** the here designated Na^+-all-solid-state coaxial standard structural battery [3]; **(2)** the coaxial cells with different CFRP tandem cork layers, A1 and A2; and **(3)** the 4 mm cork thick shell (SI, Fig. S1).

Firstly, the coaxial batteries containing the A1 cork layer performed considerably better than the ones with A2 since they exhibit higher ionic conductivity values for all four temperatures, emphasizing lower temperatures such as 0 and 10 °C (SI, Tables S1 and S3). This behavior is in agreement with the thermal insulator character of the cork. The difference between A1 and A2 layers can be explained by the fact that the A1 cork film, a more closed structure, has higher density and, therefore, is less porous, which means that it can insulate better than A2 with higher porosity and less density (SI, Table S1).

As mentioned, the standard Na^+-based all-solid-state coaxial structural battery has an ionic conductivity of 0.028 mS cm^{-1} at RT and 0.13 mS cm^{-1} at 40 °C. The different time/conditions for the experiment at 10 °C may account for a lower ionic conductivity than obtained previously at 0 °C, being a measurement of the errors involved in these experiments. The values of 0.0025, 0.0069, 0.046, and 0.15 mS.cm^{-1} obtained at 0, 10, RT, and 40 °C, respectively, show an enhancement of the ionic conductivity for the cell with the A1 cork layer when compared with the standard cell. Even for the cork layer where the improvement was not as good, A2, there is a considerable enhancement in the ionic conductivity value at 10 °C. This result can be justified by different factors: **(1)** the performance of the electrolyte is highly influenced by the absorption of moisture, and since cork works as a moisture insulator, there is no moisture absorbed by the electrolyte after fabrication, therefore leading to faster ionic conduction, especially at lower temperatures; **(2)** the cork protects the electrolyte at lower temperatures to the extent that it never allows the ferroelectric material to be at the temperature of the surroundings (sand bath or freezer), keeping it warmer; **(3)** the cork has some elasticity can contribute to a better contact in the interfaces electrode/electrolyte and therefore facilitate the conduction of ions, resulting in a lower resistance.

Our previous experience with standard all-solid-state coaxial batteries shows that the coaxial cells containing a cork layer are more stable than the standard coaxial cells since their properties remain constant for more time.

The architecture that competes with the coaxial cell with cork layer A1 has just a thick cork shell (SI, Fig. S1). The latter shows almost twice faster ionic conductivity than the one with cork layer A1 and three and a half times faster than the standard CFRP coaxial

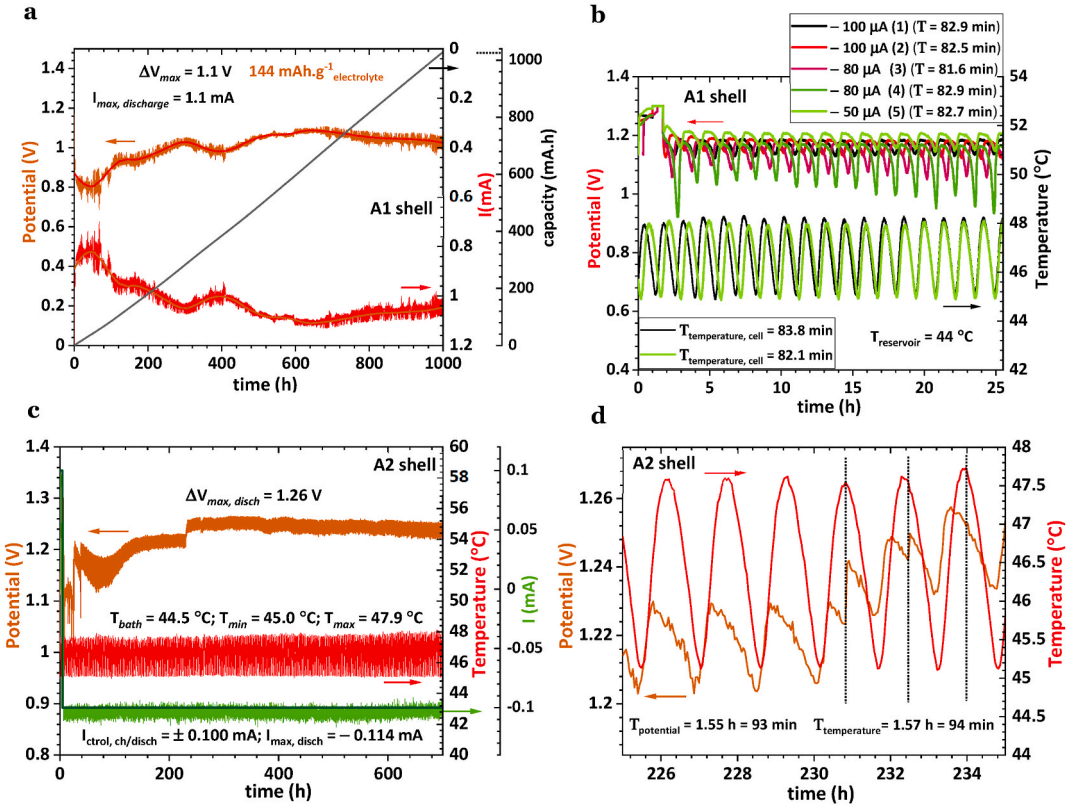

Fig. 4. A Typical discharge of an all-solid-state A1 cork coaxial structural battery connected to a 0.98 kΩ external material resistor; After the experiment in **a,** the cell was left to relax at open circuit and then in **b** made to charge at a constant current of +1 mA to 1.3 V followed by constant voltage charge at 1.3 V; discharge at a constant current of −0.1, −0.08, and −0.05 mA for 24 h; temperature oscillation is also observed and shown for charge and discharge at −0.1, and −0.05 mA; **c** cycle at constant current ± 0.1 mA of an all-solid-state A2 cork layer coaxial structural battery; the current does not show self-cycling, but the potential shows self-charge; **d** inset of **c** showing self-cycling of potential and temperature; the potential is not in phase with the temperature, it is advanced. The temperature pulsates at temperatures above the constant temperature of the sand bath where the cell is immersed. **Note**: r_a = 2 mm; r_b = 5 mm; ℓ = 95 mm (SI, 1. Materials and Methods [27–40]).

cell at 0 °C, reinforcing the initially hypothesized effect of cork at lower temperatures. Interestingly, at 40 °C, this cell is the one that performs worse, which is also expectable, as the cork does not allow the thermal equilibrium with the sand bath where the cell was submerged.

The highest values of ionic conductivity for the coaxial cell in general, 0.13 and 0.15 mS cm^{-1}, were found, as expected, at 40 °C because, as mentioned previously, the conduction of ions is highly beneficiated with an increase in temperature. Furthermore, it is anticipated that cork, as an insulator, can also protect the electrolyte long-term, reducing its degradation and preserving battery performance for extended periods.

The full discharge curve for the coaxial structural battery with an A1 cork layer demonstrates a relevant self-charging behavior previously observed for ferroelectric pouch cells and standard coaxial structural batteries [3]. The self-charge while the cell was set to discharge connected to a 0.98 kΩ material external resistor endured for more than 42 days and is shown in Fig. 4a. The capacity achieved was 144 mAh.$g^{-1}_{electrolyte}$ and 86 mAh.cm^{-2} at 1.03 V.

After the latter process, the cell was left to relax at OCV and cycled at constant voltage and current. The cell was charged at a constant current of +1 mA to 1.3 V; then at a constant potential for 45 min at 1.3 V. It was set to discharge, at a constant current of −100, −80, and −50 μA, for 24 h (Fig. 4b).

The coaxial cell self-charges at a much higher current while set to discharge with an external material resistor due to the active and nonlinear character of the ferroelectric coaxial batteries that conflict with an imposed constant current. It is demonstrated in Fig. 4b that the plateau potential does not increase with decreasing the output current from −100 to −80 μA, as expected, and as observed when the current varies to −50 μA (5th cycle shown in Fig. 4b). The coaxial battery is also able to discharge for 24 h at approximately constant average potential (SI, Fig. S3b). Likewise, the self-oscillating feature with an 82–83 min period does not depend on the output current. The cell is likely more susceptible to previous conditioning factors than to imposed output current.

The self-oscillations of the temperature behave qualitatively very similarly in all experiments shown herein.

Fig. 4(c–d) show a coaxial structural battery with A2 cork layer self-charging and self-cycling while set to cycle with a constant current of ±100 μA. The cell shows similar behavior to the A1 cork cell, as both were placed in a sand bath at approximately 40 °C. The A2 cork cell displays the self-oscillation of its temperature, measured with a thermocouple in contact with a paper sticker glued to the CFRP external surface. This detail implies that it is not the shell potential that interferes with the thermocouple, as shown hereafter, but the cell's actual temperature. The temperature is not in phase with the potential difference; it is delayed leading to conclude that a maximum in voltage conduces to a temperature rise with a subsequent maximum.

The CFRP surface did not show any potential difference when connected to the negative aluminum electrode, implying that the less dense A2 cork layer, with much lower ionic conductivity and dielectric constant, does not allow the CFRP to perform as a positive current collector.

Although the potential can be rectified to avoid the oscillating behavior, this behavior may have several applications, especially as a sensor. It is worth analyzing and understanding as a manifestation of the nonlinear character of the $Na_{2.99}Ba_{0.005}ClO$ ferroelectric-electrolyte [29], including its piezoelectric and pyroelectric properties. Moreover, temperature modulation due to the ferroelectric-electrolyte has numerous innovative applications, such as resistive metal oxide (MOX) gas sensors, thermal diodes and transistors, and memristors and oscillators for neuromorphic applications [30].

The only way the electrical potential difference in a battery cell increases while the cell is set to discharge is if the chemical potential of the negative electrode increases or the chemical potential of the positive electrode decreases, or both (by reference to the physical scale [31], where E = 0 eV for electrons at rest in vacuum). The rise in potential while sourcing a resistor is possible because there is a positive feedback flow of electrons through the electrolyte's surface. At the same time, the conduction of ions through the bulk electrolyte in the opposite direction allows for the occurrence of "limitless" cycles, portrayed by the emergent event of self-charging and self-cycling. This behavior has been systematically observed in several cells, confirming their self-charging

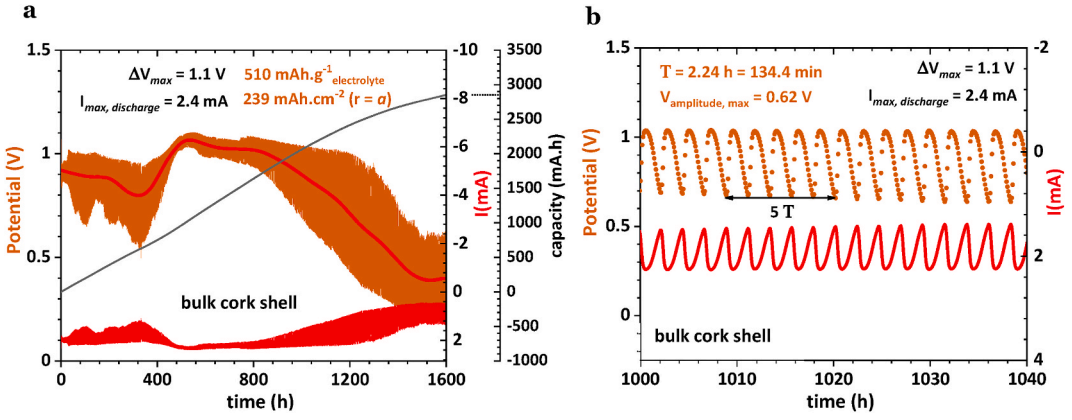

Fig. 5. Typical discharge of an all-solid-state coaxial structural battery Cu(+)/$Na_{2.99}Ba_{0.005}ClO$/Al(−) with an external thick cork shell (SI, Fig. S1) connected to a 0.46 kΩ external resistor. The cell shows self-charge and self-cycling, potentiated when the cell was set to discharge with a lower load resistor to increase the output current (≈2 mA).

capabilities [3,9].

The period of self-oscillation in Fig. 4a (A1 shell) is 98 min (SI, Fig. S3a), and in Fig. 4b (A2 shell) is 93 min.

In Fig. 5a, b, the initial OCV of 1.2 V dropped to 0.85 V when the cell was connected to the resistor, 460 Ω. The coaxial battery cell oscillated between 0.85 V and 0.83 V for ≈24 h. After this oscillating phase, the cell shows an ascending trend reaching 1.05 V. From this point, the cell displays an oscillating potential with a bigger voltage amplitude, between 0.70 V and 1.05 V with the extended period of 2.24 h, for about 150 h, i.e., six days. After this phase, the cell oscillates between lower voltage values. In this case, the cell oscillated between 0.63 V and 0.98 V. The cell's capacity, including the thick-cork shell, is 60 mAh.cm^{-2}.

It is noteworthy that the cork in the cork/Cu(+)/$Na_{2.99}Ba_{0.005}ClO$/Al(−) cell is a 4 mm thick cork cylinder casing shell (SI, Fig. S1). The thick cork cell shows approximately twice the current output than the A1 cork layer cell in Fig. 4a and SI, S3, a similar maximum potential of 1.1 V and a self-oscillation period 1.37 × its period of self-oscillating potential. Compared with another cylindrical cell, but with A2 cork, in Fig. 4(c and d), it shows 1.44 × its period. As shown in SI, Eq. (3), the capacitance is proportional to the length of the coaxial cell, and the resistance is proportional to the length's inverse SI, Eq. (1); the ratio between cells' lengths is 1.66. However, the capacitance and resistance are a function of $1/\ln\left(\frac{b}{a}\right)$, and $\ln\left(\frac{b}{a}\right)$, respectively. The $\left\{\ln\left(\frac{b}{a}\right)\right\}_{bulk\ cork\ shell} / \left\{\ln\left(\frac{b}{a}\right)\right\}_{A1\ internal\ shell}$ ratio is 1.32. Both cells with A1 and A2 cork have similar dimensions and differ only on the type of cork of the internal shell, while the radius of the cell with an external thick cork shell in Fig. 5a, b is 6.7 mm and the length 158 mm; its self-oscillations period is ~ 134 min.

In summary, increasing the radius likely extends the self-oscillation period in the same proportion. Therefore, as expected, the self-cycling phenomena are likely radial and impedance-dependent because the cell's polarization mechanisms are coaxial. It is then shown uniquely herein the inner radiuses of the ferroelectric permit controlling the self-cycling period.

Perhaps one of the most novel and exciting findings of the present study is the capacity of using a CFRP(+)/cork/$Na_{2.99}Ba_{0.005}ClO$/Al(−) cell where the Cu was also removed, Fig. 1d and 6(b, g). The CFRP accumulates the role of the external shell, mechanical protective layer, and positive collector. The advantage of this latter cell is being inexpensive while efficient with no traditional oxides-

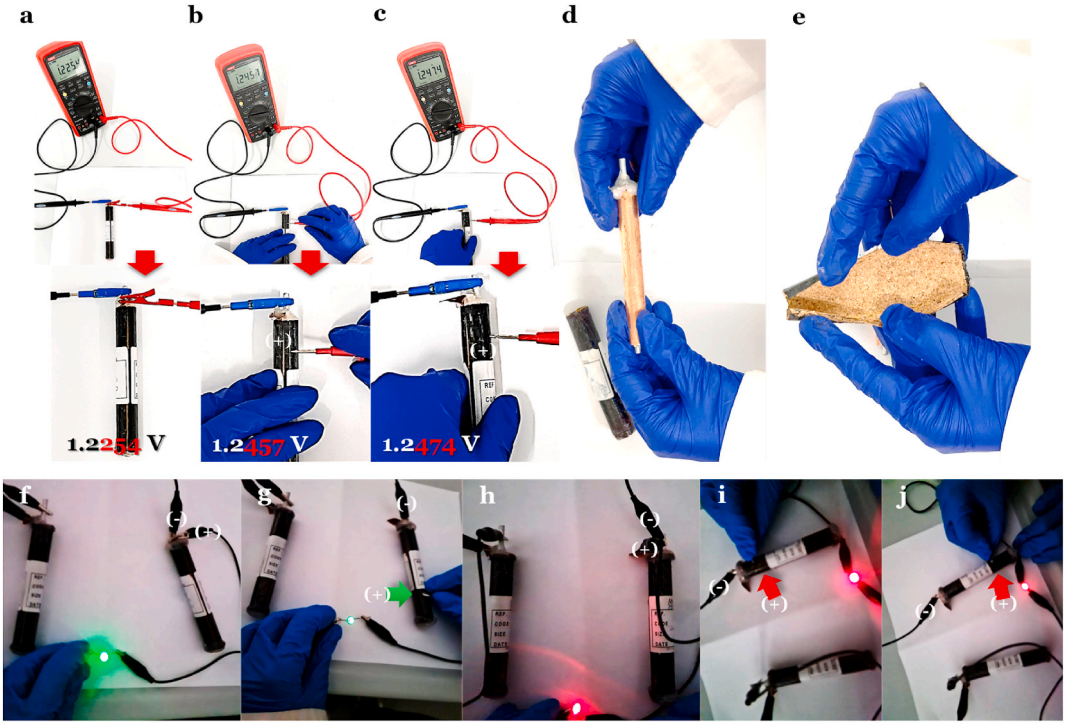

Fig. 6. All-solid-state coaxial cells open circuit voltage V_{OC} and closed circuit behavior; a CFRP/cork/Cu(+)/$Na_{2.99}Ba_{0.005}ClO$ /Al(−); b CFRP (+)/cork/$Na_{2.99}Ba_{0.005}ClO$/Al(−); c CFRP(+)/cork/Cu/$Na_{2.99}Ba_{0.005}ClO$/Al(−); d copper with the cork/CFRP shell removed showing a clean interface; e internal A1 cork layer after removal showing a clean surface (no electrolyte); Two coaxial batteries connected in series have to sum a potential higher than 1.8 V for the green LED and 1.5 V for the red LED to light the LEDs. The cell on the left is always connected through the standard collectors Cu(+)//Al(−), CFRP/cork/Cu(+)/$Na_{2.99}Ba_{0.005}ClO$/Al(−); the cell on the right is connected: f CFRP/cork/Cu (+)/$Na_{2.99}Ba_{0.005}ClO$/Al(−); g CFRP(+)/cork/$Na_{2.99}Ba_{0.005}ClO$/Al(−), CFRP(+) connected at the middle down of the cell (away from the tabs); h CFRP/cork/Cu(+)/$Na_{2.99}Ba_{0.005}ClO$/Al(−); i CFRP(+)/cork/Cu/$Na_{2.99}Ba_{0.005}ClO$/Al(−), CFRP(+) connected at the middle up of the cell; j CFRP (+)/cork/Cu/$Na_{2.99}Ba_{0.005}ClO$/Al(−), CFRP(+) connected at the middle down of the cell (away from the tabs). Note: the luminescence of the red LED is, if not as intense in h, i, and j, very similar, leading to conclude that the A1 cork layer forms a CFRP(+)/cork/Cu(−) capacitor or a CFRP (+)/cork/$Na_{2.99}Ba_{0.005}ClO$(−) capacitor enabled by the ferroelectric electrolyte that is part of the full cell CFRP(+)/cork/Cu/$Na_{2.99}Ba_{0.005}ClO$/Al (−) and CFRP(+)/cork/$Na_{2.99}Ba_{0.005}ClO$/Al(−), respectively; where Cu and $Na_{2.99}Ba_{0.005}ClO$ electrolyte surfaces have a higher surface chemical potential than the CFRP.

based electrodes that may release oxygen or being constituted of nonsustainable and expensive elements (e.g., Cobalt) or even Lithium, and, conversely, with materials that assume multiple roles.

The ferroelectric $Na_{2.99}Ba_{0.005}ClO$ provides the capacity and the topologic electronic conduction that enables the colossal electrostatic behavior of the cell, having the thick cork (1.2 mm) with a double role as dielectric and moisture and low-temperature protector for a better performance below RT.

In Fig. 6(a–c), it is demonstrated the cell CFRP(+)/cork/Cu/$Na_{2.99}Ba_{0.005}ClO$/Al(−), Fig. 6(d and e) has an OCV 22 mV, Fig. 6c, and CFRP(+)/cork/$Na_{2.99}Ba_{0.005}ClO$/Al(−) 20 mV, Fig. 6b, higher than the standard CFRP/cork/Cu(+)/$Na_{2.99}Ba_{0.005}ClO$/Al(−) cell, Fig. 6a. Both can light an LED, Fig. 6(i and j) and Fig. 6g, respectively. Fig. 6(i and j) show that CFRP(+)/cork/Cu/$Na_{2.99}Ba_{0.005}ClO$/Al (−) cell's luminescence is similar to Fig. 6h, our standard cork-layered cell where the collector is the (+) is attached to the Cu. Since the OCV of the non-standard cells is equal or slightly higher, all the differences in luminescence are due to the current and, therefore, to the coaxial cell's internal impedance.

Only with multifunctional, safe, abundant, sustainable, and inexpensive materials is it appropriate to think of actual usage for structural batteries.

3. Conclusion

Cork is introduced as a component to a multifunction system, a coaxial structural battery, to improve its performance as a protector shell and a dielectric, enabling colossal electrostatic behavior, a new valence for the cork presented in this study. More in detail, this natural material's influence on the ionic conductivity of the full cell, its permittivity, and its ability to sustain self-charge was understood. It was determined the cork could function as a dielectric in a capacitor cell architecture or enable a sustainable one-electrode-collector coaxial cell.

The present coaxial cell may pave the way for a solution for structural batteries to be used widely, as not only the current solution is safe, inexpensive, and easy to fabricate and apply. It shows a negative carbon footprint, especially as waste heat and thermal energy harvester, allows stacks in series and fabrication in various dimensions. The connection to the positive current collector placed on the wall where the battery is inserted provides for easy replacement if necessary and enables usage during winter and in colder locations of the Globe.

Contributions

Mafalda Valente: Designed and performed the experiments; Wrote the paper; Sara Magalhães Silva: Contributed materials, analysis tools and data; Maria Helena Braga: Conceived and designed the experiments; Analyzed and interpreted the data; Contributed reagents, materials, analysis tools; Wrote the paper.

Data availability

Data will be made available on request.

Conflicting interests

The authors declare no conflicting interests.

Acknowledgments

This work was supported by the Portuguese Foundation for Science and Technology FCT UIDP/50022/2020 Emerging Technologies – LAETA, and PTDC/QUI-ELT/2593/2021 "Redox-active Metal-Organic Frameworks as Electrode Materials for Lithium-Ion Batteries" projects and by the Portuguese Innovation Pact RE-C05-i01.01 | project C644936001-00000045 NGS – New Generation Storage. MHB acknowledges Professor John B. Goodenough's endowment to the MatER – Materials for Energy Research lab, FEUP. We are thankful to A. Nuno Guerreiro for performing SPK experiments and Amorim Cork Composites for providing A1 and A2 samples, expertise, and support.

Appendix A. Supplementary data

Supplementary data to this article can be found online at https://doi.org/10.1016/j.heliyon.2023.e15063.

References

[1] G.B. Olson, Science 80 288 (2000) 993–998.
[2] Y. Wang, S. Song, C. Xu, N. Hu, J. Molenda, L. Lu, Nano Mater. Sci. 1 (2019) 91–100.
[3] F. Danzi, P.P. Camanho, M.H. Braga, Molecules 26 (2021) 5226.

[4] M.H. Braga, J.A. Ferreira, A.J. Murchison, J.B. Goodenough, J. Electrochem. Soc. 164 (2017) A207–A213.
[5] S. Wang, Y. Zhang, X. Zhang, T. Liu, Y.H. Lin, Y. Shen, L. Li, C.W. Nan, ACS Appl. Mater. Interfaces 10 (2018) 42279–42285.
[6] G. Liu, J. Shi, M. Zhu, W. Weng, L. Shen, J. Yang, X. Yao, Energy Storage Mater. 38 (2021) 249–254.
[7] G.J.H. Lim, K.K. Chan, N.A.A. Sutrisnoh, M. Srinivasan, Mater. Today Sustain. 20 (2022).
[8] M.H. Braga, A.J. Murchison, J.A. Ferreira, P. Singh, J.B. Goodenough, Energy Environ. Sci. 9 (2016) 948–954.
[9] M.C. Baptista, H. Khalifa, A. Araújo, B.A. Maia, M. Souto, M.H. Braga, Adv. Funct. Mater. (2022), 2212344.
[10] L.C. Chenglong Zhao, Lilu Liu, Xingguo Qi, Yaxiang Lu, Feixiang Wu, Junmei Zhao, Yan Yu, Yong-Sheng Hu, 8 (2018) 20.
[11] M.H. Braga, Materials 14 (9) (2021) 2398.
[12] S.P. Magalhães da Silva, J.M. Oliveira, Powder Technol. 387 (2021) 16–21.
[13] J. Chanut, Y. Wang, I. Dal Cin, E. Ferret, R.D. Gougeon, J.P. Bellat, T. Karbowiak, J. Colloid Interface Sci. 608 (2022) 416–423.
[14] M.C. Lança, M. Brandt, E.R. Neagu, C.J. Dias, J.N. Marat-Mendes, J. Non-Cryst. Solids 356 (2010) 763–767.
[15] S. Paixão, C. Peixoto, M. Reinas, J. Carvalho, CEAS Space J. 14 (2022) 595–604.
[16] M. Holzinger, A. Le Goff, S. Cosnier, Front. Chem. 2 (2014).
[17] M.D. Deshpande, K. Dudley, Technical Memorandum NASA (2003) 20030055680.
[18] O. Caytan, S. Agneessens, S. Lemey, D. Vande Ginste, P. Demeester, H. Rogier, in: Proc. 2015 Int. Conf. Electromagn. Adv. Appl. ICEAA, 2015, 2015, pp. 1104–1107.
[19] J.F. Mano, N.T. Correia, J.J. Moura Ramos, B. Saramago, J. Mater. Sci. 30 (1995) 2035–2041.
[20] J. Liu, Z. Bao, Y. Cui, E.J. Dufek, J.B. Goodenough, P. Khalifah, Q. Li, B.Y. Liaw, P. Liu, A. Manthiram, Y.S. Meng, V.R. Subramanian, M.F. Toney, V. V. Viswanathan, M.S. Whittingham, J. Xiao, W. Xu, J. Yang, X.Q. Yang, J.G. Zhang, Nat. Energy 43 4 (2019) (2019) 180–186.
[21] H.S. Hirsh, Y. Li, D.H.S. Tan, M. Zhang, E. Zhao, Y.S. Meng, Adv. Energy Mater. 10 (2020), 2001274.
[22] F. Danzi, R.M. Salgado, J.E. Oliveira, A. Arteiro, P.P. Camanho, M.H. Braga, Molecules 26 (2021).
[23] L.E. Asp, K. Bouton, D. Carlstedt, S. Duan, R. Harnden, W. Johannisson, M. Johansen, M.K.G. Johansson, G. Lindbergh, F. Liu, K. Peuvot, L.M. Schneider, J. Xu, D. Zenkert, Adv. Energy Sustain. Res. 2 (2021), 2000093.
[24] J.P. Thomas, S.M. Qidwai, W.R. Pogue, G.T. Pham, J. Compos. Mater. 47 (2013) 5–26.
[25] K.J. Narayana, R. Gupta Burela, Mater. Today Proc. 5 (2018) 5580–5590.
[26] A.D.B.L. Ferreira, P.R.O. Nóvoa, A.T. Marques, Compos. Struct. 151 (2016) 3–35.
[27] L. Gil, Materials 8 (2015) 625–637.
[28] A.N. Guerreiro, B.A. Maia, H. Khalifa, M.C. Baptista, M.H. Braga (2022) 232, Batter 8 (2022) 232 8.
[29] F. Danzi, M. Valente, S. Terlicka, M.H. Braga, Apl. Mater. 10 (2022).
[30] S. Carapezzi, C. Delacour, A. Plews, A. Nejim, S. Karg, A. Todri-Sanial, Sci. Rep. 121 12 (2022) 1–9.
[31] S. Trasatti, J. Electrochem. Soc. 135 (1988) 247C.
[32] M. Maria, Incas Bull 5 (2013) 139–150.
[33] M.H. Braga, J.E. Oliveira, A.J. Murchison, J.B. Goodenough, Appl. Phys. Rev. 7 (2020).
[34] S.P. Silva, M.A. Sabino, E.M. Fernandas, V.M. Correlo, L.F. Boesel, R.L. Reis, Int. Mater. Rev. 50 (2005) 345–365.
[35] I.D.S.G. do Rosário, PhD thesis, https://fenix.tecnico.ulisboa.pt/downloadFile/563345090418603/TESE%2078560.pdf, Last Accessed: 04/03/2023o.
[36] A. Krzyzak, M. Mazur, M. Gajewski, K. Drozd, A. Komorek, P. Przybyłek, Int. J. Aerosp. Eng. 2016 (2016).
[37] Gurit, "EP 127: High TG Structural Epoxy Prepeg", https://www.gurit.com/-/media/gurit/datasheets/ep-127.pdf, Last Accessed: 03/12/2022.
[38] Alfa Aesar, "133380 Copper Foil, 0.127mm (0.005in) Thick, Annealed, 99.9% (Metals Basis)." 7440-50-8 – Copper Foil, 0.127 Mm (0.005in) Thick, Annealed, 99.9% (Metals Basis)- 13380, https://www.alfa.com/pt/catalog/013380/, Last Accessed: 4/March/2023.
[39] W.A. Zisman, Rev. Sci. Instrum. (1932) 367–370.
[40] A.N. Guerreiro, M. Baptista, B. Maia, M.H. Braga, ACS Appl. Energy Mater. (2022).
[41] J.F. Mano, J. Mater. Sci. 37 (2002) 257–263.
[42] K. Ling, M. Yoo, S. Lim, IEEE Antenn. Wireless Propag. Lett. 14 (2015) 1598–1601.
[43] R. Gonçalves, S. Rima, R. Magueta, P. Pinho, A. Collado, A. Georgiadis, J. Hester, N.B. Carvalho, M.M. Tentzeris, IEEE Sensor. J. 15 (2015) 7242–7251.